Journal of Engineering Technology and Applied Physics

Spatial Temporal Anisotropic Transport of the Microalgae *Chlorella Vulgaris* in the Microfluidic Channel

Nur Izzati Ishak* and S.V.Muniandy
Department of Physics, Faculty of Science, University Malaya, Kuala Lumpur, Malaysia.
*izzatiishak91@gmail.com
https://doi.org/10.33093/jetap.2020.2.2.1

***Abstract* - Transport of biomaterials in confined geometry exhibit complex dynamics, both in spatial and temporal scales. In this work, we examined the transport behavior of microalgae *Chlorella Vulgaris* inside the microfluidic channel under pressure-driven Poiseuille flow environment. The microalgae system is treated as the spherical naturally buoyant particles. The algae particles trajectories are visually traced using particle imaging techniques and the sample paths are resolved in streamwise (flow) and perpendicular directions. In order to understand boundary wall effects on the flow, we partitioned the microfluidic channel into three different regions, namely the center region and two near-wall boundary regions based on the velocity flow profile. Time-averaged mean square displacement (MSD), probability density function (PDF), skewness, and kurtosis of finite ensembles of particle trajectories are determined for these regions. In addition to the spatial dependencies, we also examined the transient characteristics of the algae transport at early-time and long-time. We found the existence of the mixed types for transport dynamics irrespective of flow region separation often assumed in many laminar flow simulations. This finding will be useful for optimization of mixing of algae culture in micro-scale photobioreactor as the productivity of cell growth depends critically on the cell dispersion or transport.**

Keywords—Anomalous transport, Chlorella vulgaris, microfluidic

I. Introduction

Algae are commercialized into biofuels, food and beverage, plastics, pharmaceutical, and chemical industry. Demand for algae is estimated to grow by 4.2 % from 2018 to 2025 [1]. Higher yield of algae biomass requires efficient culturing and mixing techniques, which are optimized in reactor vessel such as the photobioreactor. This type of bioreactor uses light source whether from natural or artificial and may be operated in large scales as open and closed systems. Closed systems are preferred because they provide efficient control of CO_2 and lighting, thus producing higher yields of biomass [2].

Many existing photobioreactor operate under both turbulent and laminar flow. The transition from laminar to turbulent flows or vice versa is controlled by the geometry of the reactor and the flow conditions. Reactors are specifically designed to utilize turbulent flow in order to enhance mixing and cell growth in the suspension, although the evidence of enhancement is still lacking [3]. The laminar flow is used in the air-lifts reactor to provide the mixing with help of rising bubbles, hence resulting in both cells and nutrients to disperse above the flows. It is possible to rescale the reactor into smaller sizes, where the effect of laminar flow is dominant. Interestingly, smaller dimension of photobioreactor was realized recently in PBR@ACLS photobioreactor [4] to provide food and air to the astronaut in ISS [5]. Smaller reactor provides more volumetric efficiency, minimizes the formation of biofilm that decrease the light absorption to the interior region of the flow and requires lower pumping power to drive the flow.

Transport phenomena of the bio-particles exhibit diverse characteristics due to particles complexity, interaction with media environment, flow parameters and channel geometries. For example, a pressure-driven microchannel induces the Poiseuille flow profile. This velocity profile gives rise to the non-uniform velocity across the channel, such that the occurring minimum velocity profile at the symmetrical near-wall regions and maximum velocity profile at the center region. Hence, particles driven under this type of flow will

Journal of Engineering Technology and Applied Physics (2020) 2, 2, 1: 1-9
https://doi.org/10.33093/jetap

Published by MMU PRESS. URL: https://journals.mmupress.com/index.php/jetap/index

experience different type of transport process, such as Taylor dispersion due to the drift-diffusion mechanism caused by variation in the magnitude of flow velocity across the channel width [6]. Besides, shear flow induces structural inhomogeneity in soft particles causing anisotropy in the diffusion coefficient [7]. The particles located at the near-wall boundary region will experience boundary effects, such as particle-wall interaction [8] and surface roughness interaction [9]. If the channel is too narrow, the particle will be forced to line-up in a sequence and unable for mutual passage, forming a phenomenon called single file diffusion (SFD) [10]. Additionally, under low Reynold number, the effect of media viscosity in assisting transport becomes more prominent as the viscoelastic medium causes particles to be trapped due to polymer entanglement [11, 12] and fluid heterogeneity can induce molecular crowding effect to restrict the particle motion [13, 14].

Microalgae are known to adopt a different survival mechanism in responding to a harsh environment. If the external driving force is presence, the algae are forced to move against or along the streamline. For instance, some of the algae species can perform an active transport utilizing its swimming organ (cilia or flagella) to respond to the stimulus enable it to move against, slower or faster than imposed flow [15, 16] These motile algae can swim upward on average (gravitaxis) due to bottom heaviness, having gyrating motion (gyrotaxis) due to flow gradient, biasing towards the region with rich of nutrient (chemotaxis), and light (phototaxis) [15]. As algae live in low Reynold number environment, where viscosity dominates the transport, a highly viscous environment can constraint the algae motion and the presence of the wall can further restrain its motion. Interestingly even for the non-motile algae species (absence of swimming organ), it can utilize its finite size and buoyancy to balance its position to minimize the shear effect as it gets closer to the wall. This species can develop its own active transport by manipulating its density and biofilm [17]. This active transport allows the algae to jump at a large distance over time, or moves faster than the average velocity of flow profile, or move against the streamline, or form clustering behavior.

The manipulation on the microscale environment can be realized via the microfluidic chip or it also known as the lab-on-chip. It provides a controlled microenvironment for flow profile analysis [18], mixing behavior [19], single cell analysis [20], and etc. Integrating it with the high resolution and frame video microscopy and particle tracking technique provides better insights into the mechanics of the algae transport in the microfluidic environment. Besides, the microfluidic channel can induce a confinement effect on algae transport. The general transport mechanisms present in the microfluidic environment are (1) diffusion due to collision with the fluid particle that caused the particle undergoes Brownian motion (2) drift dispersion due to the applied non-uniform velocity profile of shear flow. Combination of these two mechanisms yields drift-diffusion transport. The common way to quantify this fluctuation due to diffusion is by performing statistical moments estimation of mean square displacement (MSD) or variance, kurtosis and skewness of the probability distribution of the displacements. Some information missing from MSD estimation can be recovered from the estimation of empirical probability density function (PDF). For many particles system, average behavior of the particles is estimated by calculating the statistics based on ensemble average assumption, whereby each individual particle in the ensembles is assumed to exhibit a similar state. In the context of the transport process, the MSD is generally calculated by taking ensembles averages of square displacements at each lag time over the sample particles. This ensemble time-averaged mean square displacement (ETAMSD) method gives a reasonably good estimation of the average transport process, provided the particles in the ensemble possess can be treated as nearly identical. One must however, verify this assumption as the transport of particles under driven flow in the microchannel is non-uniform. Particles from the center region with fast motion can be transported to the boundary region or the particles can undergo slow motion due to restriction or crowding, thus introducing bias or estimation errors to the average statistics of ETAMSD.

In our early study [21], we assumed upon breaking down the particle population into subsample of two near-wall and center regions, we could estimate the sample-averaged behavior within the regions using the ETAMSD. However, careful inspection of the sample paths of the particles showed that there still exists high degree of variability in the particle transport behavior, reducing the region-based sampling size further with risk of higher inaccuracy in the ETMSD estimation. Our main objective in this study is to provide detailed analysis of the anisotropy in term of the particles' characteristics in the different regions and over time. This study will address the issues raised in the treatment of ensemble average to study average behavior of the algae particles.

The rest of this paper is organized as follows. We first introduce the transport model and Poiseuille flow dynamic in the microalgae system, then the experimental techniques used for the algae characterization, flow analysis, and particle tracking. The results and discussion are highlighted separately. Finally, a conclusion is drawn from the present study.

II. TRANSPORT MODELLING

Normal diffusion is characterized by the linear time-scaling of mean square displacement (MSD) $\langle(r^2)\rangle \sim t$, where the increments of particles displacement follow the Gaussian distribution. The deviation from the normal diffusion is called anomalous diffusion with MSD exhibits the power-law behavior:

$$\langle \boldsymbol{r}^2 \rangle = \int \boldsymbol{r}^2 P(\boldsymbol{r}, t) d\boldsymbol{r} = 2K_\alpha t^\alpha, \quad (1)$$

where $P(\mathbf{r}, t)$ is the probability of finding the particle at location $\mathbf{r}$, at time t, K_α is the generalized diffusion coefficient. The scaling exponent α is used to characterize anomalous diffusion characteristics, namely sub-diffusion for $0 < \alpha < 1$, superdiffusion for $1 < \alpha < 2$, and ballistic transport when $\alpha = 2$. Normal diffusion is recovered for $\alpha = 1$.

Two classes of stochastic processes can be used to model anomalous diffusion phenomena namely Gaussian processes and non-Gaussian processes. Gaussian anomalous diffusion such as Fractional Brownian Motion (FBM) yields a random process with the anomaly in the MSD, yet retains the Gaussian PDF property. The stochastic representation of the FBM is

$$B_H(t) := \frac{1}{\Gamma\left(H+\frac{1}{2}\right)}\left(\int_{-\infty}^{0}\left[(t-s)^{H-\frac{1}{2}} - (-s)^{H-\frac{1}{2}}\right]dB(s) + \int_0^t (t-s)^{H-\frac{1}{2}}\,dB(s)\right), \quad (2)$$

where Γ is the gamma function i.e. $\Gamma(\alpha) := \int_0^{\infty} x^{\alpha-1}\exp(-x)\,dx$ and $0 < H < 1$ is called Hurst parameter [22]. Hurst parameter H is the measure of self-similarity and is related to the anomalous scaling exponent through $\alpha = 2H$. Fractional Brownian motion $B_H = \{B_H(t): 0 \le t \le \infty\}$ produces the sample path that exhibits different degree of irregularities and two-point correlations parametrized by H. This process is used to model the fractal time series in diverse systems including, economic time series [23] and particle's motion in the viscoelastic environment [13], [24]. Another example of Gaussian model is the Scaled-Brownian motion (SBM), where the path is obtained by rescaling the Brownian motion via the non-linear time transformation [25] $t \rightarrow t_* = t^{\alpha}$, $0 < \alpha < 2$ which is used to manifests a characteristic time for the mobility variation. SBM is represented via the Langevin equation:

$$\frac{dB_S}{dt} = \sqrt{2K(t)}\xi(\tau), \quad (3)$$

with the time-dependent diffusion coefficient $K(t)$ that takes a general form [24]:

$$K(t) = K_1 t^{\alpha-1}, \quad (4)$$

where K_1 is the normal diffusion coefficient (with $\alpha = 1$). SBM is useful for modelling processes that start at origin ($X(t = 0) = 0$), without distant pass memory and found application in the water diffusion in the brain [26], and the particle's motion across the porous environment [27].

The non-Gaussian model anomalous diffusion required the violation of the central limit theorem (CLT) which guarantees the convergence of final distribution into Gaussian. This violation induces the ergodic breaking phenomena. For example, the walker undergoes the continuous-time random walk (CTWR) can encounter the trap or obstacle in their pathway causing them to be trapped with power-law waiting time PDF of the form

$$P(t) \sim t^{-1-\beta}, \quad (5)$$

where $0 < \beta < 2$. The CTRW is used to model the insulin's granule pathway across a potassium channel [28], and carrier proteins track in the plasma membrane. Another non-Gaussian model is Levy flight where the walker takes the independent increment of jump length across its pathway. The jump length l taken is characterized by the power laws PDF which can cause the divergence of moments due to heavy tail characteristics of:

$$P(l) \sim l^{-\mu}, \quad (6)$$

with $1 < \mu \le 3$ [29]. When $\mu = 1$, the transport shows the ballistic (deterministic) behavior and $\mu = 3$ exhibits more Brownian motion. When $\mu < 3$, the path follows the anomalous diffusive behavior, where its second moment diverges ($\langle l^2(t)\rangle \rightarrow \infty$). For $\mu < 2$, the first moment is divergent ($\langle x(t)\rangle \rightarrow \infty$). These divergences of moments are due to heavy tail characteristics of the distributions where the particle may experience extremely long jumps. The summation of the independent and identically distributed (iid) random variables with divergence variance leads to the generalized central limit theorem, where the limit of this distribution is characterized by α-stable Levy distribution [29]. Hypothetically, biological organism's pathway will adapt to the Levy's flight in optimizing their random search translation for the food, nutrients, territory, and etc [30].

III. Methodology

A. Algae Culture Preparation

The *Chlorella Vulgaris* culture is grown in Bold's Basal medium (BBM) at a pH of 6.6 under controlled-environment incubator at a temperature of 28 °C. The detailed characterization of algae culture can be found in the study [21].

B. Experimental Setup

The experimental set-up is prepared as shown in Fig. 1. The set-up includes a pressure controller, a flow sensor, an input reservoir, an output reservoir, a Y-junction microfluidic chip with channel's width and height of 250µm and 200µm respectively, a high-speed CCD camera with a zoom lens, and high-power LED source (not shown). The induced flow in this system is a stable and pulseless pressure-driven flow. A pressure and flow controller are used to regulate and stabilize the input pressure generated from the compressor. The coupling between pressure controller and flow sensor is applied to produce the feedback loop, so that constant flow rate of the fluid entering the inlet can be maintained. To ensure constant flow rate throughout the experiment, we monitored the feedback of the fluctuation of pressure and flow rate on a computer with aids of ESI Microfluidic Software (ElveFlow). The particle tracking experiment is done within periods of 24 hours after we first obtained a fresh algae culture.

The particle tracking experiment is performed using a bright-field microscope technique. A mirror tilted into angle of 45° is placed underneath the microfluidic stage to reflect the light from the LED source, so that this light can be collected by the objective lens and coupled to CCD camera. As a result, the algae specimen object appeared dark against the white background.

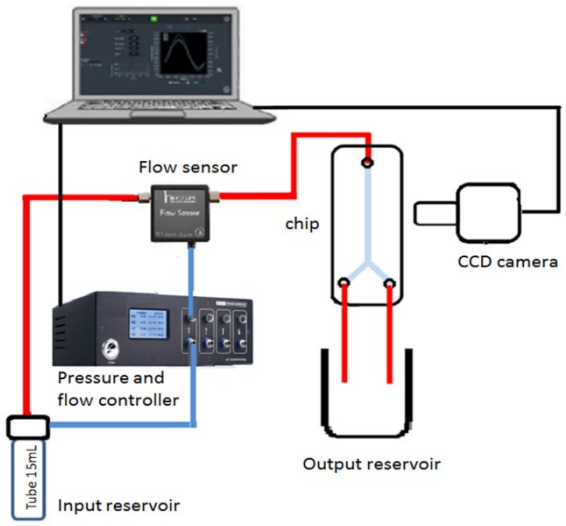

Fig. 1. Microfluidic flow experiment schematic.

C. Microfluidic Flow Experiments

We first pumped the deionized water and then BBM solution into the channel with a high flow rate of $3000\ \mu L/\text{min}$ to remove unwanted suspension or contamination inside the channel. The algae suspension in BBM solution inside the input reservoir is pressurized before we set the particles free at a specific flow rate of $0.2\ \mu L/min$ by controlling the pressure between inlet and outlets via the pressure controller (OB1 Elvesflow). This flow rate is chosen for its stability. The flow is maintained for 10 minutes to ensure the uniform flow across the microchannel. Approximately at a distance of L = 2.1 cm away from the channel inlet, the image of the particle's motion is recorded and captured via the Mikrotron CCD camera with a frame rate of 2000 frame per second (fps). The high-power LED source is used to illuminate the background into appropriate brightness. The choice of frame rate used is balanced by compensating the speed of flow and accessible light illumination available in this tracking experiment.

D. Particle Tracking Experiment

At the distance of L = 2.1 cm from the channel's inlet, the Poiseuille flow is assumed to be fully developed in the microchannel. Imposing this type of flow in a rectangular microchannel, the velocity flow profile exhibits minimum value at the near-wall boundary regions, while shows maximum value near the center area. Thus, the particles driven under this flow will be transported at the different rates based on the inheritance of velocity profile at the specific on the flow regions as shown in Fig. 2. Based on the above argument, we grouped the particle according to the region of profiles: (1) near wall boundary NB_1, (2) near-wall boundary NB_2, and (3) center region C. The flow regions are roughly estimated by using the Segré-Silberberg radius as the reference point [31], [32]. This radius estimates the average equilibrium position of the particle's migration as 60 % from the center plane. In the case of a symmetrical rectangular channel of width and height of $250\ \mu$m and $200\ \mu$m respectively with references to channel's hydraulic radius of R , the approximate equilibrium position r_{eq} is 75 μm. Then, the approximate length of NB_1, NB_2 and C are given by $50\ \mu\text{m} < r_{eq_{b1}} < 0\ \mu\text{m}$, $175\ \mu\text{m} < r_{eq_{b2}} < 250\ \mu\text{m}$ and $50\ \mu m < r_{eq_c} < 175\ \mu m$ respectively.

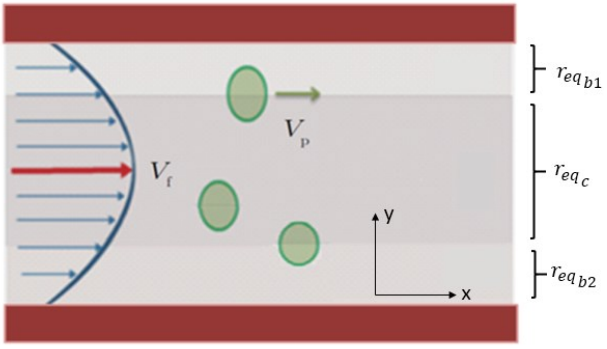

Fig. 2. Simple classification of the flow regions into near wall boundary NB_1 and NB_2 regions (lighter shaded area), and center region C (darker shaded area). The particle travelled with velocity V_p under influenced of the fluid velocity profile V_f.

The reference plane of analysis is defined with respect to the direction of flow, such that x-plane corresponds to the streamwise (longitudinal) direction and y-plane is the perpendicular (transverse) direction. The trajectory of individual particle is constructed using Fiji plugin algorithm [33, 34] that link a particle in one field image to the most probable closest particle in the next field image. The particle field has the link to the next particle field if the distance travelled is less than inter-particle spacing. The trajectory that is not germane in analysis such as "fake" particles is discarded by the imposition of constraint in average velocity, track's duration, and the number of spots. Additionally, the presences of immobile particles that may stick in the z-direction's upper wall are also eliminated from the final analysis. To refine the accuracy of the tracked particle, we resampled the stack video images into five smaller sample stacks. The first 1000 frames are omitted analysis.

IV. Results

A. Trajectories

The particles are transported according to the streamline paths with different behaviors such as restrictive motion with high fluctuation and small step size (Fig. 3(a)), Gaussian-like pathway (Fig. 3 (c)), and the track with larger step size (Fig. 3 (b)). Interestingly, these paths are observed across the entire channel's region. All of the particle paths are influenced by drift from the applied flow. The observed oscillations are due to the drift in the x-direction (streamwise). In fact, without the drift the algae still able to move with zero mean displacement.

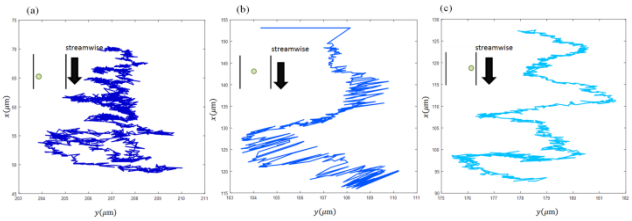

Fig. 3. The representative sample of particle tracks taken at the region of (a) NB_1, (b) C , and (c) NB_2.

In the pressure-driven flow, the algae transport system is influenced by the environment consisting of flow and fluctuation. The applied flow on the system via the pumping the fluid under constant pressure creates uniform drifts across the channel length. All of the algae particles have the tendency to follow the drift induced by the flow. On the other hand, the fluctuation of the environment caused the algae to be transported with wiggles. The drift hides the fluctuation of algae trajectory as shown in Fig. 4, where the apparent particles paths exhibit persistent tracks.

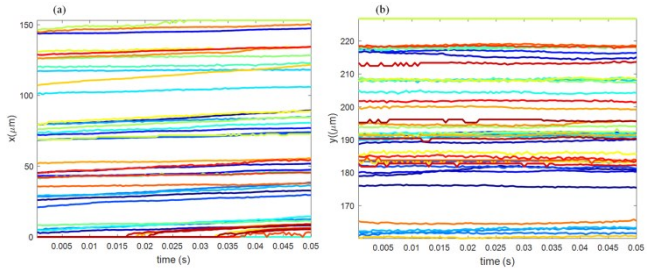

Fig. 4. Sample trajectories of particles resolved in (a) x-direction (streamwise) and (b) y-direction (perpendicular).

By de-trending operation i.e. removing the mean drift from data set, we essentially removed the drift trend. Once the

drift is removed, the particles oscillate more in the y-direction (perpendicular) than in x-direction (streamwise). The fluctuation of the particle trajectories are now made more visible for the investigation of the diffusion characteristics. For a drift-diffusion process such as in microfluidic channels, the drift may overwhelmed the particles transport. If the drift term is removed by de-trending, the particle fluctuations can be analyzed using statistical moments and probability distribution function.

Pressure-driven flow caused motion in streamwise direction to exhibit more persistent /deterministic trend with small fluctuation as illustrated in Fig. 5 (a). On the other hand, both shear stress and diffusion cause noticeable fluctuation (Fig. 5 (b)) on the trajectories of algae in the perpendicular direction.

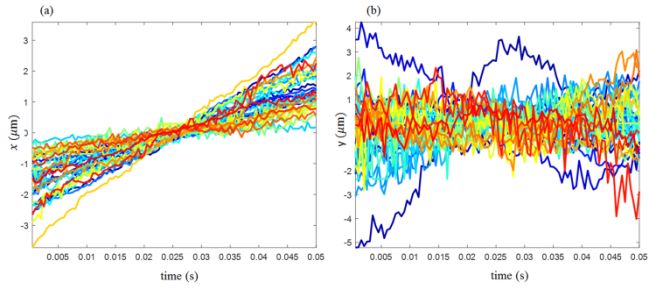

Fig. 5. Detrended sample trajectories of particles (a) x-direction (streamwise) and (b) y-direction (perpendicular).

B. Mean Square Displacement

The variance or essentially mean square displacement (MSD) is calculated by resolving the MSD components into streamwise (x-component) and perpendicular (y-component) directions. A quarter of overall data points are utilized in computing the time average mean square displacement (TAMSD) $\langle \bar{\delta}^2 \rangle$ at the lag time τ over trajectory $r(t)$ on length M:

$$\langle \overline{\delta^2}(\tau) \rangle = \frac{1}{1-\tau} \int_0^{M-\tau} [r(t+\tau) - r(t)]^2 dt \,, \qquad (7)$$

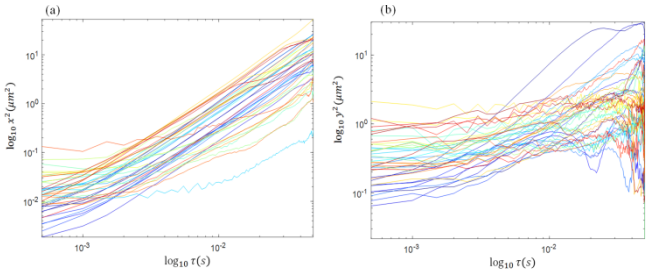

Fig. 6. Log–log plots of TAMSDs of individual particle trajectories against lag time in (a) the streamwise (x-component) and (b) perpendicular (y-component) directions.

The individual plots of TAMSD are shown in Fig. 6. Different scaling behaviors (slope) of TAMSD are observed between the short and long lag-times over a period of decade. Following our previous work [21], the scaling exponent at lag-time of $t < t_c$ and $t > t_c$ where t_c is the transition time are extracted by imposing the linear least square regression on the bi-logarithmic TAMSD curve . The slope derived from the curve is corresponding to the scaling exponent of α_1 and α_2 at the short and long lag-time, respectively.

Figures 7-9 illustrate the distributions of TAMSD scaling exponents estimated from particle trajectories for the near-wall boundary regions of NB_1 and NB_2 and the center C at the streamwise (blue) and perpendicular (red) directions. In the streamwise direction, at earlier and later times (Fig. 7 (a, b), Fig. 8 (a, b), and Fig. 9 (a, b)), the distribution of the MSD scaling exponents of α_1 and α_2 are skewed to the right with high frequency of particles exhibiting strong superdiffusive motion ($1 < \alpha < 2$). While in the perpendicular direction (Fig. 7 (c, d), Fig. 8 (c, d), and Fig. 9 (c, d)), the MSD scaling exponents distributions at both time regimes are skewed to the left with larger frequency of particle transported in the subdiffusive motion ($0 < \alpha < 1$). The tendency of having broad type of transport motion in streamwise and perpendicular directions imply the existence of the anisotropic transport among the particles in all regions.

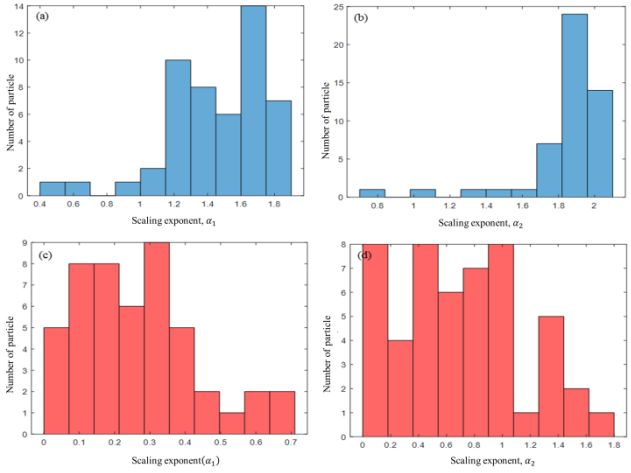

Fig. 7. Distribution of the MSD scaling exponents in the near wall boundary NB_1 region at streamwise (a, b) and perpendicular (c, d) with the scaling exponent α_1 at the shorter lag time (a, c) and α_2 longer lag time (b, d).

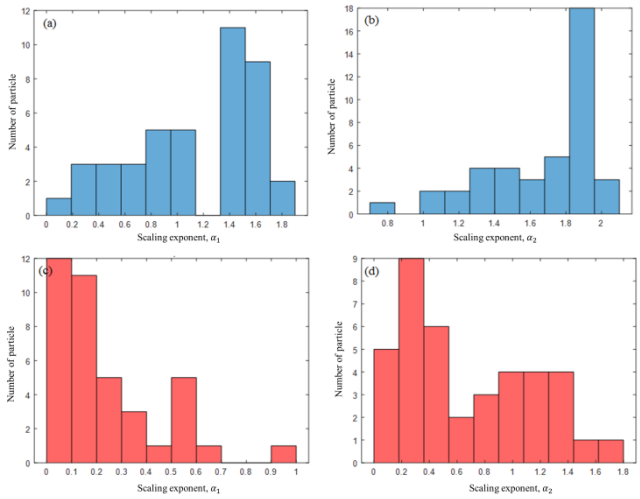

Fig. 8. Distribution of the MSD scaling exponents in the near wall boundary NB_2 region at streamwise (a, b) and perpendicular (c, d) with the scaling exponent α_1 at the shorter lag time (a, c) and α_2 longer lag time (b, d).

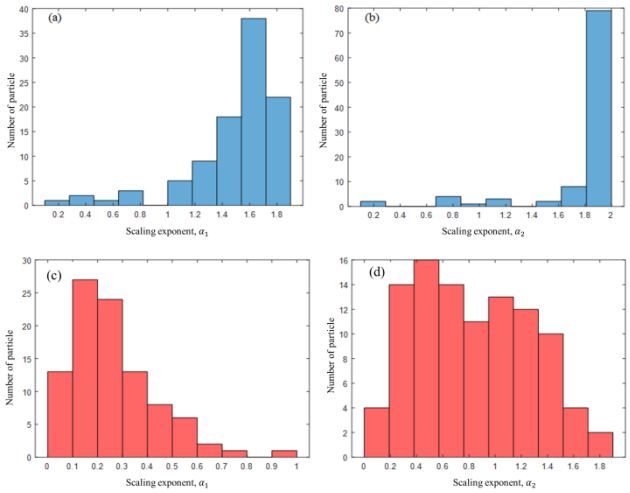

Fig. 9. Distribution of the MSD scaling exponents in the center C region at streamwise (a, b) and perpendicular (c, d), with the scaling exponent α_1 at the shorter lag time (a, c) and α_2 longer lag time (b, d).

We summarize the percentage of occurrence of mixed transport characteristics observed in the sample of 63 particles in Table I. In the streamwise direction at the earlier time of transport in the boundary region of NB_1, 94.0 % of the particle undergoes superdiffusion and only 6 % transported in subdiffusion. While at a later time, reveals the majority of 84.0 % of the algae transported in superdiffusive and 12.0 % performed ballistic transport and a small minority of 4.0 % of particle undergoes subdiffusion. At the perpendicular direction (see Table II), majority of the particle's bias for slow subdiffusive transport at the earlier lag time and at the later time, while 76.0 % of the particle undergoes subdiffusive, and 24.0 % exhibit the faster transport. These show that the degree of heterogeneity is increased at a later time. In the case of boundary region NB_2 at the streamwise direction of an earlier time (see Table I), 65.0 % of particles undergo superdiffusion and 35.0 % transported in subdiffusion. At the latter time, majority of the particles (93%) transported in the superdiffusion. For the perpendicular direction (see Table II), majority of the particles exhibit subdiffusion in earlier time while at later time 74.4 % of algae particles exhibit subdiffusion, 25.6 % experience superdiffusion. In the center region C at the streamwise component skewed to the right with the majority of 92.9 % particles showed superdiffusive transport. In the latter time, majority of the particles remained superdiffusive. In the perpendicular direction, in earlier time all the algae transported in fully subdiffusive mode. In a later time, the majority of 66.0 % the particles transported in subdiffusion and remaining 34.0 % with superdiffusion.

Table I. Percentage of particle's contribution to MSDs scaling exponent distribution in streamwise component.

Streamwise (x)	Percentage of particle (%)				
	α_1		α_2		
	$0 < \alpha_1 < 1$	$1 < \alpha_1 < 2$	$0 < \alpha_2 < 1$	$1 < \alpha_1 < 2$	$\alpha_2 = 2$
NB_1	6.0	94.0	4.0	84.0	12.0
NB_2	35.0	65.0	2.5	92.9	4.6
C	7.1	92.9	7.1	80.8	12.12

Table II. Percentage of particle's contribution to MSDs scaling exponent distribution in perpendicular component.

Perpendicular (y)	Percentage of particle (%)				
	α_1		α_2		
	$0 < \alpha_1 < 1$	$1 < \alpha_1 < 2$	$0 < \alpha_2 < 1$	$1 < \alpha_1 < 2$	$\alpha_2 = 2$
NB_1	100	0	76	24	0
NB_2	100	0	74.4	25.6	0
C	100	0	66	34	0

The MSD scaling exponents' distributions clearly showed the spatial-temporal anisotropy in the transport of algae particles in the microfluidic channel. The degree of anisotropy is highest in the streamwise direction at both time regimes and in the perpendicular direction at a long lag-time in both near-wall regions. Assuming uniformity in particle transport by simple stratification of near-wall and center regions may not be valid in such systems.

C. Probability Density Function

The typical way of analyzing transport behavior is by using MSD. As the particles transport in this system has high degree of variability i.e. the particles do not move in the same rate, the usage of MSD may be inaccurate. To compensate for uncertainty, we computed the empirical probability density function (PDF) of the particles' displacement at different time-lags and results are shown in Fig. 10 (a-f). The number of bins to compute the PDF is obtained by using the Freedman-Diaconis rule by averaging the optimal number of bins for individual displacement in lag-time.

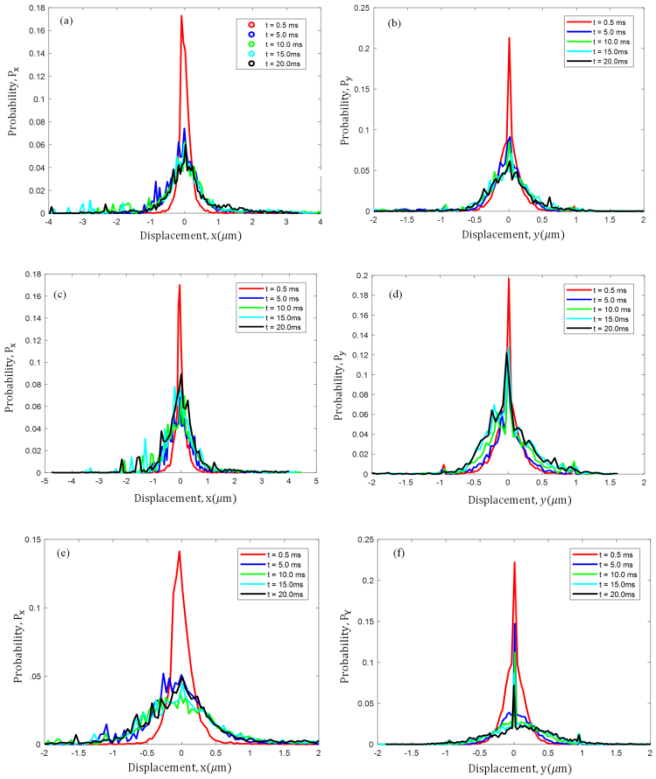

Fig. 10. Empirical probability density distribution function of particles in streamwise components (a, c, e) and perpendicular direction (b, d, f). The PDF are shown for NB_1 (a,b), NB_2 (c, d) and C (e, f) region, respectively at different lag-times $\tau = 0.5\ ms$ (red), 5.0 ms(blue), 10.0 ms (green), 15.0 ms (sky blue), and 20.0 ms (black).

The empirical PDF showed sharp peaks at the origin and heavy tail characteristics, which imply non-Gaussianity at small lag-time ($t \sim 0.5$ ms) in all flow regions for both components of particle trajectories. At the short-time interval, the particles have the tendency to be immobilized as indicated by the sharp peak at the origin and to displace with very small magnitude. However, this non-Gaussian feature is retained only for small time-lag. As the particles move at longer times, the distribution of particle displacements (at t = 10.0 ms, 15 ms and 20.0 ms) spread with the decrease in distribution peak, followed by the formation of heavy tails. Noting the MSD scaling exponent distribution in streamwise and perpendicular direction (Figs. 7–9), particles with strong subdiffusive motion, strong superdiffusive motion or ballistic can alter the tail of the distribution at many scales, which induce flow heterogeneity.

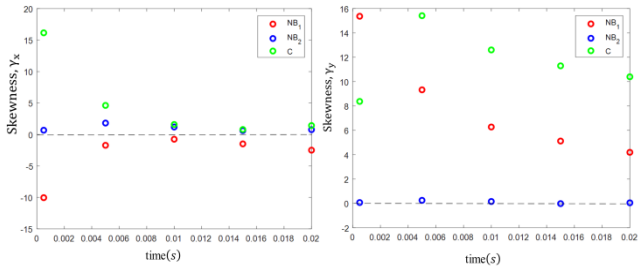

Fig. 11. Skewness of the particles displacement as a function of lag time in (a) streamwise(x) direction and (b) perpendicular direction(y) at near wall boundary regions NB_1(blue circle), NB_2(red circle), and center C (green circle).

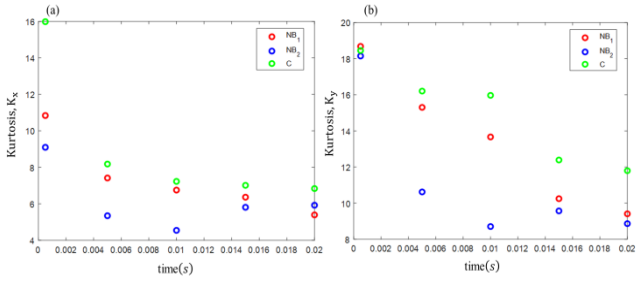

Fig. 12. Kurtosis of particles displacement as a function of lag time in (a) streamwise(x) direction and (b) perpendicular direction(y) at near wall boundary regions NB_1(blue circle), NB_2(red circle), and center C (green circle).

Further characterization of the distribution is done by computing the skewness and kurtosis of distribution curves, as shown in Fig. 11 and Fig. 12, respectively. The time evolution of the empirical distributions of microalgae displacement in flow regions NB_1, NB_2 and C show high magnitudes of skewness and kurtosis as compare to the normal distribution that has skewness ($\gamma = 0$) and kurtosis (k = 3.0). As shown in Fig. 11 (a), the distribution of particle displacements in the perpendicular (y) direction has negative skewness, which means the particle spreads more to the left. Meanwhile, in the streamwise direction (Fig. 11 (b)), the distribution has positive skewness value as particle spreads more to the right. However, as the lag-time increases, the skewness of the distribution decreases i.e. approaches zero, which indicates the system approaches symmetric normal distribution in long time limit. At the initial time and in both x- and y-directions, the algae displacements showed asymmetry in the PDFs. The asymmetry decreases and becomes more symmetric as lag time increased.

V. DISCUSSIONS

Algae particles transport in microfluidic are shown to be both nonstationary and spatial anisotropic. The temporal dynamics can be described using MSD analysis with cross-over time t_c that enables the characterization of the particles' displacements at different time regimes. At the early time of $t < t_c$, the particle's inertia causes it to perform the slow dynamic. As $t > t_c$, the particles velocity approach that of the fluid flow. During this excursion period, the paths of the particles show strong fluctuation. This dynamic is the result of the mismatch of the particle's velocity to the flow's velocity. Even the small mismatch of this velocity can caused the emergence of stagnation point in flow [35]. At early time, the particle takes time to overcome its inertia before it can be transported according to the local flow.

At the streamwise direction in near boundary region of NB_2, the percentage of the particles experience the subdiffusion motion at earlier time is higher as compared to its symmetrical counterpart of the NB_1 .This implies the particles mechanics in these boundary regions are not symmetric, which is inconsistent with our first assumption of symmetrical Poiseuille flow profile. While at the later time, percentage of particle exhibit subdiffusion are reduced while more particles get transported in superdiffusion, indicating the particles in NB_2 and NB_1 regions sharing the similar mechanics at the long time scale as indicated by unimodal distribution of MSD scaling exponents at with peak occurs at strong superdiffusion. The temporal non-symmetrical behavior of the majority of the particles at early time is caused by instabilities of local flow. The perfect symmetry of the theoretical Poiseuille flow is not achieved in our experiment because of local flow variation. Another possible explanation is the existence of the stronger stagnation or fluid recirculation at NB_2 regions causing more particles to be trap. The observation of higher percentage of particles in superdiffusion mode in NB_1 compared to NB_2 is resulted from some particles from center region C can migrate quickly to NB_1 region inducing the large number of particles undergo superdiffusion in NB_1 region.

At center region C in the streamwise direction, the percentage of particles undergo subdiffusion remained the same at all time regimes. This can be explained by the particle-hydrodynamic interaction, which can reduce the MSD scaling exponent/diffusivity. A numerical study [36] showed that a small portion of the immobile particles can have strong effect on the remaining fraction of particles through the hydrodynamic and drag interactions. Through particle imaging, we observed a small fraction of immobile microalgae at short time interval (this particle is removed during tracking and sampling process). These immobile particles can reduce the mobility of its neighbors through hydrodynamic effect. The fact that both boundary regions and the center region C share approximately same percentage of particles undergoing three modes of transport i.e. subdiffusion, superdiffusion, and ballistic at later time indicated that particles from center region can migrate to the boundary region and vice versa. This phenomenon is observed by [31], where the particles in rectangular channel undergo lateral migration with rate/degree of its transverse depends on its interaction with the environment.

The distribution of the MSD scaling exponents at the perpendicular direction exhibits almost bimodal distribution

at the NB_1 and NB_2 region with major peak occurs at the strong subdiffusion and second peak at weak subdiffusion, while at later time, the major peak at the subdiffusion and minor peak at superdiffusion (see Fig. 7 (c, d) and Fig. 8 (c, d)). This indicates heterogeneous transport at the boundary regions causing the particles within this boundary to interact with shear and boundary effect at different strength depending on the local position i.e. nearer to the wall boundary or center region boundary. In the center region C, the distribution of the MSD scaling exponent (Fig. 9 (c, d)) showed unimodal distribution as particles experienced slow transport due to shear flow only. However, the occurrence of peak of MSD scaling exponent at strong subdiffusion range implied that even for the particle that far away from the boundary region can experience strong restricted motion. The slow motion of the particles can be related to caging effect imposed by the neighboring particles through the particle-hydrodynamic effect or crowded environment.

In the perpendicular direction, a greater number of particles in all respective flow regions of undergoes the subdiffusion transport at the early time and transits to slightly fast transport in the later time. Before the transition occurs, the particle can bounce back and forth within the cage imposed by the neighboring particles as illustrated in the sharp peak of empirical PDF (see Fig. 10). The particle's motion at this regime is heavily influenced by the cooperative motion of its immediate neighbors, which known as "collective relaxation". As the surrounding particles relax the imposed "cage" on a central particle, then the particle is able to transport in fast motion. The temporal slow transport behavior at the early time is also associated to the thermal motion in viscoelastic medium. The viscoelastic properties induced the caging effect on the particle pathway causing the anti-correlation displacement of the particle [37]. The transition time take place at $t_c \sim 0.03$ s is corresponding to the rheology and speed of the flow. There is also a possibility that the particle slowing down at earlier time as it backscattered from the collision between other particles, before it drifted back by the drift flow [38]. However, we observed no collision took place in our system, where the particle appeared to pass one another. Thus, the caging effect is most likely induced the anisotropy in particle transport.

The *Chlorella vulgaris* is an "active" particle as it can alter the local environment releasing its respiratory waste products as extracellular polymeric substances (EPS). The EPS can alter the pH value of the environment, by raising the acidity of the environment over time [39]. In fact, the EPS can be released in form of the biofilm that loosely attaches to cell wall as survival mechanisms in stress environment [40]. This process can induce the heterogeneity behavior as each alga possesses different mass, density, and diameter. The temporal anisotropic transport can emerge as the viscosity of local environment changes over time.

The empirical PDF at the early lag time shows the high peak and long tail distribution at all flow regions and components wise. The sharp peak at the displacement distribution in streamwise components is caused by fraction of particle displaced with extremely small displacement from the origin as shown in strong subdiffusion. While in perpendicular direction, the sharp peak is contribution from majority of the particles undergo subdiffusion. Thus, the peak of PDF is sharper at the perpendicular direction as compared to the streamwise direction where the particles have higher tendency to immobilize or displaced with extremely small magnitude in spatial perpendicular component. This is caused by the restriction of available space for the particle to interact with the local flow due to presence of wall. Additionally, the high drag force exerted at the normal-wall direction further reduces the average displacement taken by the particle. In long time, the particle can displace more as the fluctuation arises from the wall effects and flow instabilities subside at the later time. From the estimation of the empirical TAMSD, PDF plot, skewness, and kurtosis we found that the algae particles exhibit non-Gaussian behavior at early time and diminished at longer time in all regions. However, this non-Gaussian behavior was not sustained as the evolution of empirical PDF at the later time approached Gaussian features.

VI. CONCLUSION

The transport of microalgae in the microfluidic channel exhibits highly transient and anisotropic characteristics, which cannot be treated as stratified flow with respect to near-wall boundaries and center regions across the channel width. There seemed to be mixed slow and fast dynamics in all the regions. A simplified analysis which based on clustering of particle behavior with respect to the regional profile of Poiseuille flow may not be accurate. Within a sub-region, we observed a broad distribution of the scaling exponents of particles in both components wise which correspond to heterogeneity transport. These results are useful for the design of efficient bioreactor to meet the throughput and flow requirement. If natural anisotropic transport under laminar flow in very small Reynold number can be induced, then turbulent flow is not necessary to induce mixing of algae culture.

ACKNOWLEDGEMENT

This work is partially supported by University Malaya Faculty Research Grant (GPF035B-2018) and Fundamental Research Grant Scheme (FP057-2014A). The authors thank Professor S.M. Phang and Dr. F.L. Ng at the Institute of Ocean and Earth Sciences (IOES), University of Malaya for their assistance in algae culture and suggestions.

REFERENCES

[1] A. Kadam, "Algae Products Market by Type (spirulina, chlorella, astaxanthin, beta carotene, and hydrocolloids), Source (brown algae, blue-green algae, red algae, and green algae), Form (solid and liquid), and Application (food & beverages, nutraceuticals & dietarys)". Retrieved from: https://www.alliedmarketresearch.com/algae-products-market.

[2] L. G. Ramirez-Merida, L. Q. Zepka and E. Jacob-Lopes, "Current Status, Future Developments and Recent Patents on Photobioreactor Technology," *Recent Patents Eng.*, vol. 9, no. 2, pp. 80–90, 2015.

[3] O. Croze, G. Sardina, M. Ahmed, M. Bees and L. Brandt, "Dispersion of Swimming Algae in Laminar and Turbulent Channel Flows : Consequences for Photobioreactors," *J. R. Soc. Interface*, vol. 10, no. 81, pp. 1–14, 2013.

[4] H. Helisch *et al*, "Non-Axenic Microalgae Cultivation in Space – Challenges for The Membrane µgPBR of the ISS Experiment PBR @ LSR," in *48th International Conference on Environmental Systems*, pp. 1–12, 2018.

[5] M. Johnson, "Building Better Life Support Systems for Future Space Travel," 2019. Retrieved from : https://www.nasa.gov/mission_pages/station/research/news/photobioreactor-better-life-support.

[6] M. Latini and A. Bernoff, "Transient Anomalous Diffusion in Poiseuille Flow," *J. Fluid Mech.*, vol. 441, pp. 399–411, 2001.

[7] X. Cheng, X. Xu, S. Rice, R. Dinner, and I. Cohen, "Assembly of Vorticity-aligned Hard-sphere Colloidal Strings in A Simple Shear

Flow," *Proc. Natl. Acad. Sci.*, vol. 109, no. 1, pp. 63–67, 2012.
[8] K. Yeo and M. R. Maxey, "Anomalous Diffusion of Wall-bounded Non-colloidal Suspensions in A Steady Shear Flow," *Europhys. Lett.*, vol. 92, no. 2, pp. 24008–24014, 2010.
[9] T. Fehr and H. Lowen, "Glass Transition in Confined Geometry," *Phys. Rev. E*, vol. 52, no. 4, pp. 4016–4025, 1995.
[10] P. S. Burada, P. Hänggi, F. Marchesoni, G. Schmid and P. Talkner, "Diffusion in Confined Geometries," *ChemPhysChem*, vol. 10, no. 1, pp. 45–54, 2009.
[11] A. Godec, M. Bauer and R. Metzler, "Collective Dynamics Effect Transient Subdiffusion of Inert Tracers in Flexible Gel Networks," *New J. Phys.*, vol. 16, no. 9, pp. 18–20, 2014.
[12] W. You and W. Yu, "Slow Linear Viscoelastic Relaxation of Polymer Nanocomposites : Contribution from Confined Diffusion of Nanoparticles," *Macromolecules*, vol. 52, no. 23, pp. 9094–9104, 2019.
[13] J. F. Reverey, J.H. Jeon, H. Bao, M. Leippe, R. Metzler and C. Selhuber-Unkel, "Superdiffusion Dominates Intracellular Particle Motion in The Supercrowded Cytoplasm of Pathogenic Acanthamoeba Castellanii," *Sci. Rep.*, vol. 5, pp. 11690–11704, 2015.
[14] K. Julius, J. Weine, M. Gao, J. Latarius, M. Elbers, M. Paulus, M. Tolan and R. Winter, "Impact of Macromolecular Crowding and Compression on Protein − Protein Interactions and Liquid − Liquid Phase Separation Phenomena," *Macromolecules*,vol. 52, no. 4, pp. 1772-1784, 2019.
[15] R. Rusconi, J. S. Guasto and R. Stocker, "Bacterial Transport Suppressed by Fluid Shear," *Nat. Phys.*, vol. 10, no. 3, pp. 212–217, 2014.
[16] R. Rusconi and R. Stocker, "Microbes in Flow," *Curr. Opin. Microbiol.*, vol. 25, pp. 1–8, 2015.
[17] A. M. Roberts, "Mechanisms of Gravitaxis in Chlamydomonas," *Biol. Bull.*, vol. 210, no. 2, pp. 78–80, 2006.
[18] F. J. Tovar, P. Thurgood, C. Gilliam, T. Nguyen, E. Pirogova, K. Khoshmanesh and S. Baratchi, "A Microfluidic System for Studying The Effects of Disturbed Flow on Endothelial Cells," *Front. Bioeng. Biotechnol.*, vol. 7, no. 81, pp. 1-6, 2019.
[19] C. D. Tsai and X. Lin, "Experimental Study on Microfluidic Mixing with Different Zigzag Angles," *Micromachines*, vol. 10, no. 583, pp. 1-14, 2019.
[20] T. Luo, L. Fan, R. Zhu and D. Sun, "Microfluidic Single-Cell Manipulation and Analysis : Methods and Applications," *Micromachines*, vol. 10, no. 104, pp. 1-31, 2019.
[21] N. I. Ishak, S. V Muniandy, V. Periasamy, F. L. Ng and S. M. Phang, "Anisotropic Transport of Microalgae *Chlorella Vulgaris* in Microfluidic Channel," *Chinese Phys. B*, vol. 26, no. 8, p. 088203, 2017.
[22] B. B. Mandelbrot and J. W. van Ness, "Fractional Brownian Motions , Fractional Noises and Applications," *SIAM Rev.*, vol. 10, no. 4, pp. 422–437, 1968.
[23] B. B. Mandelbrot, *Fractals and Scaling In Finance: Discontinuity, Concentration, Risk*, 1st ed. Springer Publishing Company, Incorporated, 2010.
[24] J. H. Jeon, A. V Chechkin and R. Metzler, "Scaled Brownian Motion: A Paradoxical Process with A Time Dependent Diffusivity for The Description of Anomalous Diffusion.," *Phys. Chem. Chem. Phys.*, vol. 16, no. 30, pp. 15811–7, 2014.
[25] S. C. Lim and S. V. Muniandy, "Self-similar Gaussian processes for Modeling Anomalous Diffusion," *Phys. Rev. E - Stat. Nonlinear, Soft Matter Phys.*, vol. 66, no. 2, pp. 1–14, 2002.
[26] D. S. Novikov, J. H. Jensen, J. A. Helpern and E. Fieremans, "Revealing Mesoscopic Structural Universality with Diffusion," *Proc. Natl. Acad. Sci. U. S. A.*, vol. 111, no. 14, pp. 5088–5093, 2014.
[27] P. N. Sen, "Time-dependent Diffusion Coefficient As A Probe of Geometry," *Concepts Magn. Reson. Part A*, vol. 23A, no. 1, pp. 1–21, 2004.
[28] S. M. A. Tabei, S. Burov, H. Y. Kim, A. Kuznetsov, T. Huynh and J. Jureller, "Intracellular Transport of Insulin Granules Is A Subordinated Random Walk," *Proc. Natl. Acad. Sci.*, vol. 110, no. 13, p. 4911–4916, 2013.
[29] G. M. Viswanathan, E. P. Raposo and M. G. E. Luz, "Lévy Flights and Superdiffusion in The Context Of Biological Encounters and Random Searches," *Phys. Life Rev.*, vol. 5, no. 3, pp. 133–150, 2008.
[30] G. M. Viswanathan, S. V Buldyrev, S. Havlin, M. G. E. da Luz, E. P. Raposo and H. E. Stanley, "Optimizing the Success of Random Searches," *Nature*, vol. 401, no. 6756, pp. 911–914, 1999.
[31] Y.L. Chen, "Inertia- and Deformation-driven Migration of A Soft Particle in Confined Shear and Poiseuille Flow," *RSC Adv.*, vol. 4, no. 34, pp. 17908–17916, 2014.
[32] A. Gupta, L. Chow, R. Kumar and A. Ladd, "Effect of Aspect Ratio on Inertial Migration of Neutrally Buoyant Spheres in A Rectangular Channel," in *47th AIAA Aerospace Sciences Meeting*, pp. 1–14, 2009.
[33] J. Schindelin *et al*., "Fiji: An Open-source Platform for Biological-Image Analysis," *Nat Meth*, vol. 9, no. 7, pp. 676–682, 2012.
[34] J.Y. Tinevez *et al*., "TrackMate: An Open and Extensible Platform for Single-Particle Tracking," *Methods*, vol. 115, pp. 80–90, 2016.
[35] J. H. E. Cartwright, U. Feudel, G. Károlyi, A. de Moura, O. Piro and T. Tél, "Dynamics of Finite-Size Particles in Chaotic Fluid Flows," in *Nonlinear Dynamics and Chaos: Advances and Perspectives*, M. Thiel, J. Kurths, M. C. Romano, G. Károlyi and A. Moura, Eds. Berlin, Heidelberg: Springer Berlin Heidelberg, pp. 51–87, 2010.
[36] S. J. Bussell, D. L. Koch and D. A. Hammer, "Effect of Hydrodynamic Interactions on The Diffusion of Integral Membrane Proteins: Tracer Diffusion in Organelle and Reconstituted Membranes," *Biophys J*, vol. 68, no. 5, pp. 1828–1835, 1995.
[37] M. A. Despósito and A. D. Viñales, "Subdiffusive Behavior in A Trapping Potential: Mean Square Displacement and Velocity Autocorrelation Function," *Phys. Rev. E - Stat. Nonlinear, Soft Matter Phys.*, vol. 80, no. 2, pp. 1–7, 2009.
[38] U. Balucani, J. P. Brodholt and R. Vallauri, "Analysis of The Velocity Autocorrelation Function of Water," *J. Phys. Condens. Matter*, vol. 8, no. 34, pp. 6139–6144, 1996.
[39] Y. S. Z. Fan and C. C. X. Xu, "An Auto-flocculation Strategy for Chlorella Vulgaris," *Biotechnol. Lett.*, vol. 37, no. 1, pp. 75–80, 2014.
[40] L. Liu, G. Pohnert and D. Wei, "Extracellular Metabolites from Industrial Microalgae and Their Biotechnological Potential," *Mar. Drugs*, vol. 14, no. 191, pp. 1–19, 2016.